Chemical Engineering Journal 477 (2023) 146926

Contents lists available at ScienceDirect

Chemical Engineering Journal

journal homepage: www.elsevier.com/locate/cej

Reactor design for thin film catalyst activity characterization

Cham Trinh [a,*], Yangjun Wei [a], Anupam Yadav [a], Martin Muske [a], Nico Grimm [b], Zehua Li [c], Lukas Thum [a], Dirk Wallacher [b], Robert Schlögl [c], Katarzyna Skorupska [c], Rutger Schlatmann [a], Daniel Amkreutz [a]

[a] PVcomB / Helmholtz-Zentrum Berlin für Materialien und Energie GmbH, Berlin, Germany
[b] Department Sample Environments / Helmholtz-Zentrum Berlin für Materialien und Energie GmbH, Berlin, Germany
[c] Fritz-Haber-Institut der Max-Planck-Gesellschaft, Faradayweg 4-6, Berlin 14195, Germany

ARTICLE INFO

Keywords:
Reactor design
Thin film catalyst
CFD modelling
Virtual replica
Chemical reaction modelling
Direct current electrical heating

ABSTRACT

Thin film-based systems hold enormous potential for atomic-scale control of catalysts and their supports. So far, there is only limited reactor design with dedicated characterization methods for such catalyst systems. Thus, this work focuses on designing and prototyping a tailored reactor to characterize thin films catalysts. Herein, an electrically driven reactor and its virtual replica are designed together in a way to measure and describe the reaction processes over thin film catalysts. The developed numerical model comprised of coupled fluid-, thermal-, and chemical reaction models in combination with the well-defined geometry of the prototype allows a fast and comprehensive testing of novel catalysts systems, which is illustrated by acetylene hydrogenation with a palladium based thin film catalyst on silicon substrates as first model reaction. A power law model was found to be most appropriate to describe the kinetics of the corresponding reaction. It is shown that the codesigned virtual replica offers a strong platform for comprehensive testing and fairly accurate description of thin film catalysis.

1. Introduction

Thin-film technology has proven to allow for both: atomistic control of bulk and surface of materials, as well as easy and economic upscaling. This is impressively reflected in photovoltaics, where the current solar cell records [1] would not be possible without a perfect understanding and control of interface-state density and bulk quality on the one hand and up-scaling the technology to 500GW/a in 2021 (PV-magazine) on the other hand [2]. The transfer of this principle to catalysis shapes the core mission of the CatLab project [3], in which the development and production of tailored, thin-film catalysts are the main focuses.

Up to now spray coating, impregnation or sintering are the main technologies for large volume catalyst production [4,5], on the lab-scale nano particle growth is intensively studied [6], but due to the high complexity of the deposition methods, up-scaling is challenging. The formation of thin films is precisely controllable in crystallography, composition and homogeneity, suitable for research both in small and large scale since it is a well-understood technology [7,8], but applying this approach to catalysis demands new reactor concepts to study the catalytic properties of these layer systems.

There are limited reactor designs with dedicated characterization methods for thin-film catalyst. A variety of catalytic characterization systems which are designed for powders or monoliths are mostly packed-bed reactors [9], and few of them own very rare design concepts (e.g., Jet-Loop). Some studies of thin film catalyst characterisation were conducted in tubes utilizing a conventional furnace as heat source [10–12]. However, it is challenging to assess the dead volume and evaluate the correct temperature on surface of samples [13]. Micro-channel reactors and monolith reactors prepared by wash coat method have showed advantages to circumvent this, with high surface to volume factor, suppression of hot spots and low pressure drop, high conversion and selectivity [12,14–19]. In both types of reactors, the thickness of the catalyst films on reactor walls is μm scale but are not specified for catalyst characterization. The monolithic electropromoted reactor [20,21], a hybrid between honeycomb monolithic reactor and plate flow cell, is for screening thin film catalyst with the advantage of flexibility in assembly and dismantling of catalyst coated substrates. Microreactors as demonstrated by Srinivas et al. [22] offer low dead volume, high surface to volume ratio, but the fabrication is complex due to photolithography or polymer synthesis technology [23]. Moreover, the heating supplies of the previously described reactors are conventional furnaces or cartridge heaters [14,22,24,25], neglecting an inherent advantage of thin-film

* Corresponding author.
E-mail address: cham.trinh@helmholtz-berlin.de (C. Trinh).

https://doi.org/10.1016/j.cej.2023.146926
Received 16 February 2023; Received in revised form 18 October 2023; Accepted 23 October 2023
Available online 25 October 2023

Fig. 1. Scheme of simulated reactor with the configuration of triple circular nozzles. Si substrates are displayed as violet colour and the grey one is the inner of reactor.

catalysts: energy efficient and fast heating by deposition of catalysts on electrical conductors allowing for direct current electrical heating, which is the heating concept of the approach described in this paper.

In this work, a reactor design for thin film catalyst activity characterization is proposed. Our reactor concept aims to maximise catalytic surface area and achieve homogenous reaction conditions by low temperature and pressure gradients, easy fabrication, handling and adaption to various reaction conditions or analytical instrumentation.

2. Concept and design rules

nm-thick thin film catalyst, which is deposited on substrates (so called catalyst plates), is the main object of our work. To characterize our catalysts the reactor design is proposed to:

(1) maximize the active area meaning A(cat) / A(total) = 1 and minimize dead volume.
(2) provide gradient free operation (radial concentration, temperature, radial flow velocity, pressure etc.).
(3) well-defined geometries to allow rigorous coupling to numerical modelling.

Based on this proposal, a small channel design with symmetric face-to-face catalyst plates was envisioned. The small cross section is able to fulfil requirement (1) and (2): the dead volume around the corner of the reactor is eliminated by the round corner design to maximize the active catalytic area, and the symmetric narrow cross-section enables homogenous characterisation conditions and avoid uneven temperature distribution. And the long channel allows long gas residence time for characterization. In our design, length and width of reactor was chosen as 5 cm × 1 cm with a variable spacing of the catalyst plates. According to this well-defined and robust geometries, the 3-D modelling were then done to prove the concept, fulfilling requirement (3). More details are given in the following sections.

Side walls are designed as frame structures with gas-inlet and outlet nozzles located at the short sides of the structure. This offers a high level of modularity, since the frame is exchangeable and can be further tailored to match a variety of reaction conditions, channel widths or nozzle geometries. For this concept channel design, nozzle configuration and diameter have to be optimized to maximize the interaction between feed gas and catalyst surface. Particularly, nozzle configuration and size, catalyst plates distance play an important role in generation of dispersion [26,27], which is caused by turbulent regime next to inlet nozzles, and can improve the mixing of feed gases and enhance gas interaction with the top and bottom catalytic surface. But since homogenous reactions are required throughout the whole reactor, the conditions of formation of this turbulent region and extension needs to be understood and should be as small as possible.

Additionally, our heating concept, which is direct resistive heating of the catalyst plates, is included in the numerical model to investigate the temperature profile of the reactor. The direct current electrical heating provides a fast and accurately controlled temperature during reaction. Due to the fast response, temperature deviations can be compensated quickly. Finally, to investigate the chemical reaction properties, a surface reaction rate-based model is implemented as described in the following section.

3. Simulation method

We used COMSOL Multiphysics [28] as a platform to simulate the processes in the designed reactor. Details of the mesh of the simulation model is given in Fig. A1. As mentioned before, we employed 3 physical domains to create a virtual replica of the prototyped reactor: computational fluid dynamics (CFD) for gas flow and distribution simulation, heat transfer and finally a basic chemical reaction model (transport of concentrated species) based on surface rate equations. The scheme of 3D-simulated device is shown in Fig. 1. The governing equation, model assumption and related boundaries are listed in Table 1 and 2.

The gas flow inside reactor was first modelled to study the influence of nozzle configuration and the reactor geometry on the flow. Three configurations were investigated: slit nozzle, single circular, and triple circular nozzles (Fig. 3a). The influence of gas channel height (spacing between the face-to-face catalyst plates) on gas flow was also investigated. The simulations were performed using the properties of nitrogen as feed gas in this simulation.

Laminar flow, which is described by the Navier-Stokes equation, was used to model the flow in the reactor for low and medium flow rates. At high flow rates of feed gas (>150 ml/min), a turbulent region evolves at the entrance and a refined turbulent model was employed to simulate the flow accordingly. Slip at boundaries was neglected for this

Table 1
Governing equations.

Navier Stokes	$\rho(\frac{\partial u}{\partial t}+u\nabla u) = -\nabla p + \nabla\cdot\left(\mu\left(\nabla u+(\nabla u)^T\right)-\frac{2}{3}\mu(\nabla\cdot u)I\right)$	**Nomenclature**
Reynolds Averaged Navier Stokes	$\rho(\frac{\partial \boldsymbol{u}}{\partial t}+\boldsymbol{u}\nabla\boldsymbol{u}) = -\nabla \boldsymbol{p} + \nabla\cdot\left((\mu+\mu_T)\left(\nabla\boldsymbol{u}+(\nabla\boldsymbol{u})^T\right)-\frac{2}{3}(\mu+\mu_T)(\nabla\cdot\boldsymbol{u})I\right)$	ρ: gas density u: velocity
Continuity equation	$\frac{\partial\rho}{\partial t}+\nabla(\rho u) = 0$	**u**: time-average velocity p: pressure
Transport equation	$\frac{\partial}{\partial t}(\rho\omega_i)+\nabla\bullet(\rho\omega_i\boldsymbol{u}) = -\nabla\cdot\boldsymbol{j}_i + R_i$ $\boldsymbol{j}_i = -\rho D_i\nabla\omega_i$	**p**: time-average pressure μ: dynamic viscosity μ_T: dynamic viscosity
Heat transfer	$\rho C_p\frac{\partial T}{\partial t}+\rho u C_p\cdot\nabla T+\nabla\cdot q = Q_{vd}$ $q = -k\nabla T$ $Q_{vd} = \tau:\nabla u$	I: identity tensor $\mathbf{j}_i$: mass flux D_i: diffusivity of specie i R_i: reaction rate of specie i ω_i: mass fraction of specie i T: temperature k: thermal conductivity C_p: heat capacity *q*: heat flux Q_{vd}: viscous dissipation τ: viscous stress tensor

Table 2
Boundary condition.

	CFD	Transport concentrated species	Heat transfer
Initial condition	$u = 0$, p = 0	$w_{0,i} = 0$	T = 297.3 K
Inlet	Fully developed flow:$u = u_0$	$w_i = w_{i,0}$	$T = T_{in}$
At wall	No slip:$u = 0$	On Si (boundary flux-surface reaction): $-n{\cdot}J_i = J_{0,i}$; Other walls (no flux):$-n{\cdot}J_i = 0$	On Si surface, constant temperature according to testing conditions:$T = T_{const}$
Outlet	$p = p_{out}$	$n{\cdot}\rho_i{\cdot}D_i\nabla w_i = 0$	

Table 3
Kinetic parameters from literatures for Pd foil taken from [37–39].

Parameter	A	x	y	E_a (kJ/mol)	$A_{s,c}$ (m^2/mol)
Value	5×10^6	1.04	−0.66	40	1.26×10^4

Table 4
Kinetic parameters from literatures for Pd/ γ-Al_2O_3 taken from [40].

Parameter	A_1	A_2	A_3	A_s (m^2/kg)
Value	$759.2 \times exp(\frac{-1215}{T})$	$6.74 \times exp(\frac{1732}{T})$	3.95	350

simulation. The inlet condition was set by mass flow rate. At the outlet, back pressure is equal to working pressure (i.e., gauge pressure).

For direct current electrical heating concept, the resistivity of the silicon substrate is 1.5x10^{-2} Ωcm. Temperature dependent heat capacity and thermal conductivity of Si [29,30] were considered. Since the direct current electrical heating provides a fast and accurately controlled temperature during reaction (see Fig. A2), a constant-temperature boundary on the Si surfaces is considered in Table 2.

Chemical reaction modelling was performed to provide an assessment on catalytic performance of the catalyst material in this reactor. The transport of the reaction species was simulated by transport of concentrated species model [28], which was coupled with laminar flow to evaluate the mass transport. The surface reaction was modelled as flux of reactive species onto the catalyst surface and product flux leaving the catalyst surface.

For our chosen model reaction, namely acetylene hydrogenation, the reaction pathway including first the conversion to ethylene and to ethene subsequently is described by:

$$C_2H_2 + H_2 + AS(ads) \rightleftarrows C_2H_4 + AS(ads) \quad (1)$$

$$C_2H_4 + H_2 + AS(ads) \rightleftarrows C_2H_6 + AS(ads) \quad (2)$$

where, AS(ads) is the surface element, which is set to constant concentration during kinetic simulation of the reaction. In this simulation, acetylene is assumed to first be converted to ethylene, as shown in Eq. (1), and other products are formed by the consecutive reactions, similar as Eq. (2). This means for the evaluation of the conversion, only Eq. (1) was taken into account in the simulation and the conversion results will be compared with experimental tests, while the selectivity is not considered in the simulation due to the lack of thin-film characterisation in the literature.

There are various models to study the kinetic mechanisms for this reaction, which are described in literature [30–37], and they are not developed directly based on thin-film catalysts. Nevertheless, considering that a catalyst supported in different forms of substrates is likely to behave similarly due to same intrinsic kinetic mechanism, we assume that some of these reaction rates of acetylene can be adapted to our first reaction model for thin-film catalysts. In this work, we used two models to simulate kinetic data. First, a model created for palladium foils [38,39]; and second, a model for Pd supported on γ-Al_2O_3 developed by Bos et al. [40].

For the case of a Pd foil, the reaction rate (consumption rate of acetylene) is based on a power-law model and is written as [38]:

$$-r_{C_2H_2} = A \times P_{H_2}^x \times P_{C_2H_2}^y \times exp\left(\frac{-E_a}{RT}\right) (\text{reactions/site/s}) \quad (3)$$

where the constant values (pre-exponential factor A, reaction orders x and y) were determined by fitting the experimental data of Pd foil and listed in Table 3. P_{H_2} and $P_{C_2H_2}$ are the partial pressures of hydrogen and acetylene respectively. E_a is activation energy and R, T are Boltzmann constant and temperature, respectively. The reaction rate is determined by the unit reactions per active site per second or turn over frequency (TOF). The total number of active sites on the surface is assumed to be equal to surface concentration ($A_{s,c}$-mol/m^2) of metal atoms multiplied with the site occupancy number of acetylene on a Pd surface [28,41]. For the first study, site occupancy number is assumed to be 1, meaning one acetylene molecule adsorbs on one Pd surface atom, thus the surface reaction rate will be:

$$r_{C_2H_2,s} = r_{C_2H_2} \times A_{s,c} (\text{mol/m}_2\text{/s}) \quad (4)$$

where $A_{s,c}$ is taken from literature [37] and listed in Table 3.

The model from Bos et al. [40], derived by CO poisoning studies on Pd nanoparticles on alumina, holds validity for feeds with or without CO in the feed gas. The rate expression based on the Langmuir-Hinshelwood type mechanism can be simplified for the case without CO to:

$$-r_{C_2H_2} = \frac{A_1 P_{C_2H_2} P_{H_2}}{(1 + A_2 P_{C_2H_2}) \times (1 + A_3 P_{H_2})} (\text{mol/kg}_{\text{cat}}\text{/s}) \quad (5)$$

where, A_1, A_2, A_3 are experimentally fitted terms listed in Table 4.

One should note that this model was developed for pellet catalysts. The unit of the reaction rate is therefore mol/kg_{cat}/s. In order to adapted it to thin-film catalyst, in this work, the surface reaction rate for the gas C_2H_2 is assumed to equal to the reaction rate for the gas C_2H_2 per mass divided by the active metal surface (A_s-m^2/kg_{cat}):

$$r_{C_2H_2,s} = \frac{r_{C_2H_2}}{A_s} (mol/m^2/s) \quad (6)$$

An overview of all parameters for kinetic simulations is provided in Table 4. Thus, the simulated conversion of the reaction is calculated as:

$$\chi_{C_2H_2,simulated} = \frac{n_{C_2H_2,in} - n_{C_2H_2,out}}{n_{C_2H_2,in}} \quad (7)$$

where, $n_{C_2H_2,in}$ and $n_{C_2H_2,out}$ are the total mole flow (mol/s) at inlet and outlet, respectively.

4. Experimental methods and catalyst preparation

4.1. Pressure drop and heating experiment

Pressure drop inside the reactor is one of the most important integral factors to assess gas phase processes inside the reactor. Low pressure drop indicates a low gradient in gas concentration, enabling a homogenous concentration of the reactants over the whole reactor, thus this parameter was determined experimentally using the manufactured prototype as shown in Fig. 2 and correlated to the developed CFD model. Before the actual pressure drop measurement, the reactor was filled with nitrogen until a steady state was reached. During measurements, the

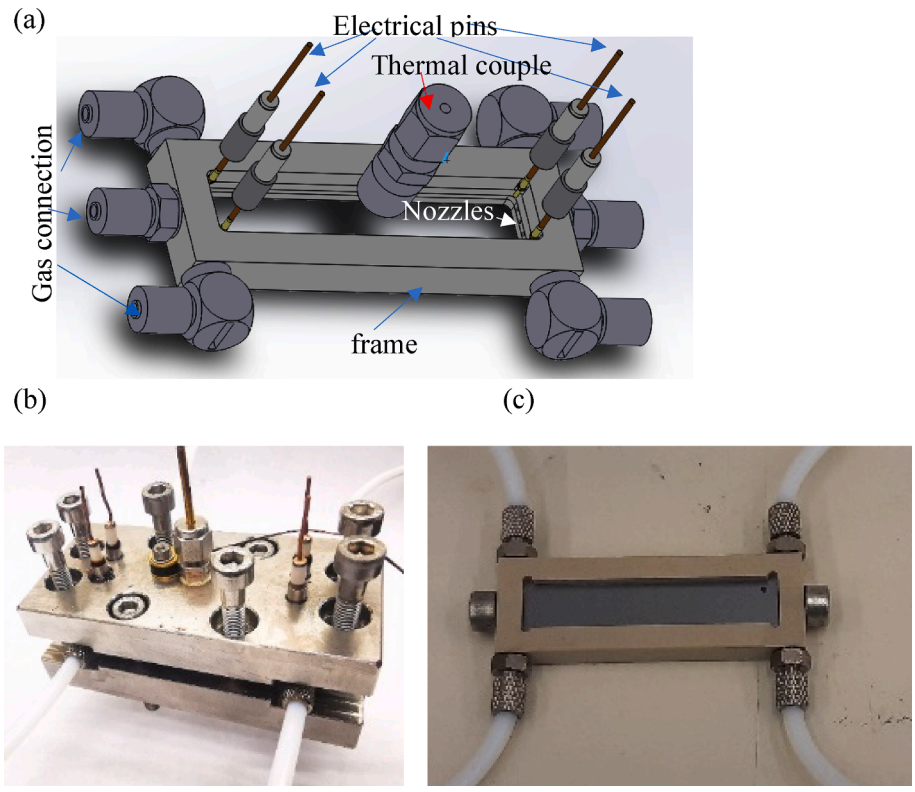

Fig. 2. (a) 3D sketch of body reactor with structuring frame, 4 metal roots are for electric power connecting and one connection (in middle) for thermocouple. (a) Manufactured reactor with housing (b) manufactured reactor body assembled Si wafer. The frame of reactor body is made by PEEK. The reactor is symmetric both in flow and cross-section directions, so the assignment of inlets/outlets can be either side.

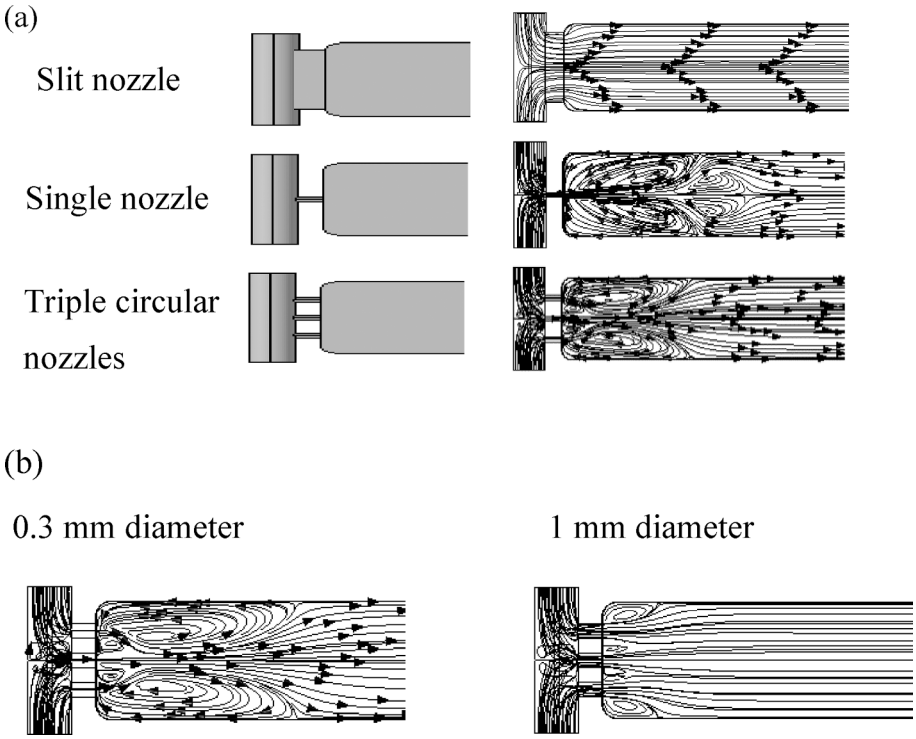

Fig. 3. (a) (Left) 2D image of simulated device and (Right) Streamlines in case of slit nozzle, single and triple circular nozzles. (b) Streamlines in 2D view for reactor with 0.3- and 1-mm nozzle diameter. Simulations were done with channel height of 1 mm, the flow rate of 140 ml/min, operating pressure of 1 bar and at room temperature.

Table 5
Testing condition.

Test	Pressure drop	Heating	Catalysts Activity	
			High conversion condition	Low conversion condition
Pressure(bar)	0.5–1.25	1	1	1
Temperature (^{o}C)	Room Temperature	100	30,50	19.5–50
Gas	N_2	N_2	C_2H_2, H_2, N_2	C_2H_2, H_2, N_2
Flow rate (ml/min)	30–350		33.7	134.8
Mole ratio C_2H_2: H_2: N_2			1:30:6.5	1:10:26.5
Pd area (cm^2)			10	5

back pressure was controlled at a constant value, and the volumetric flow rate (at standard condition) of N_2 feed gas was varied from 10 to 350 ml/min. The experiment was conducted at room temperature. Pressure drop was determined as difference between pressure gauge readings at inlet and outlet port. The back pressure itself was varied from 0.5 to 1.25 bar.

Integrated electrical heating was implemented in this reactor design. Identical catalyst plates were directly connected to a constant current source in series, thus same temperatures are expected for both. The temperatures were measured by thermal couples touching the rear of the catalyst plates at their centre position. An asymmetric heating test, in which only one Si wafer was heated, was performed additionally to examine differences in temperature between these two wafers. Due to the thermal limitation of the frame material (Polyether ether ketone (PEEK)) for the first manufactured prototype, the target temperature is set to100 ^{o}C for the test.

4.2. Catalysts preparation and catalytic testing

A 200 nm thick SiN_x film was deposited on doped ($1.5x10^{-2}$ Ωcm) Si

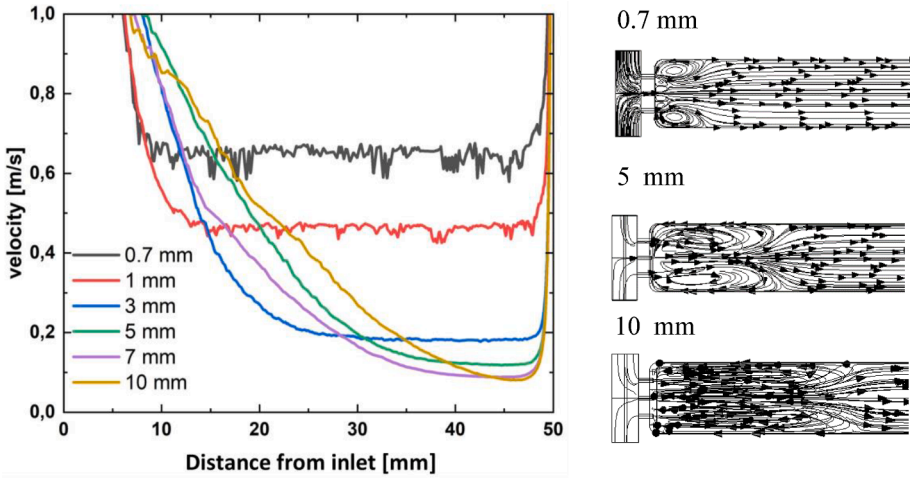

Fig. 4. Velocity distribution along reactor at different reactor height (distance between plates). Simulations were done with the flow rate of 140 ml/min, operating pressure of 1 bar and at room temperature.

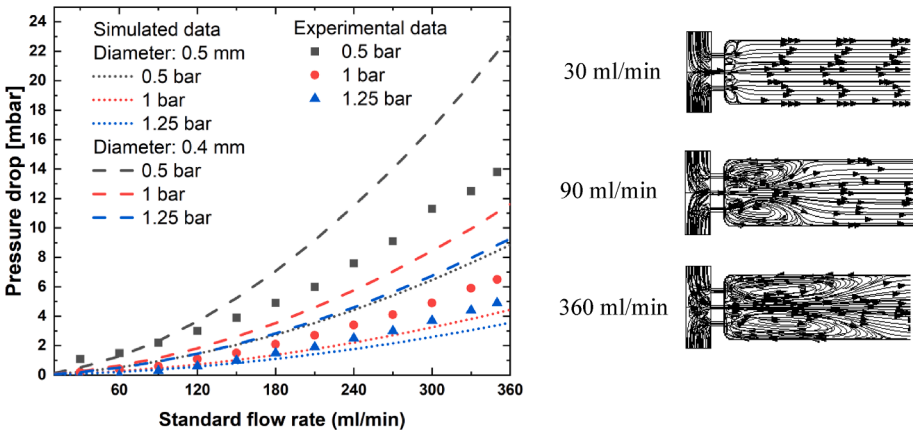

Fig. 5. (Left) Pressure drops vs standard flow rate of the feed gas with triple circular nozzles. Pressure drop was determined as difference between pressure gauge readings at inlet and outlet port, and standard flow rate of the feed gas is given at standardized conditions (ambient temperature, absolute pressure 1 atm). Working pressures in the reactor of 0.5, 1 and 1.25 bar are marked in the graph as black, red and blue colours. (Right) The streamlines for standard volumetric flow rate of 30, 90 and 360 ml/min at operating pressure of 1 bar and room temperature. Simulations were done with channel height of 1 mm, the flow rate of 140 ml/min, operating pressure of 1 bar and at room temperature.

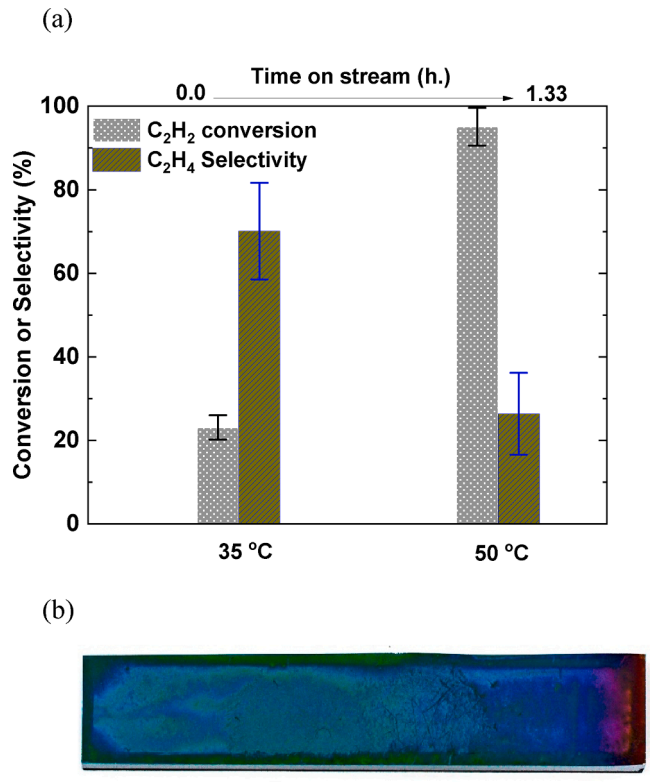

Fig. 6. (Top) Conversion and selectivity in case of two Pd/SiN_x/Si substrates at operating temperature of 35 and 50 °C. (Bottom) Si sample after the test. The left side of Si is near the inlet. Experimental condition is shown in Table 5 for the high conversion cases.

substrates (5 × 5 cm) by a plasma enhanced chemical vapor deposition. Afterwards, 3 nm palladium as catalyst was deposited by magnetron sputtering and tested under acetylene hydrogenation reaction conditions. Since there exists air contact between these two depositions, there might be a SiN_x layer contaminated by a small fraction of oxygen. Before catalytic testing, a blank test was performed by installing bare silicon substrates in the reactor. First, argon was purged into the reactor for 30 min at 80 °C, followed by a gas mixture comprising C_2H_2, H_2 and N_2. The gas composition at the outlet was analysed by a gas chromatograph (GC, Agilent 7890) equipped with a capillary column and a flame ionization detector (FID). Under these conditions, a negligible acetylene consumption could be detected.

Two catalyst coated plates were installed in the reactor, as shown in Fig. 1. A total feed flow rate of 33.7 ml/min with 2.67 % of acetylene was used (C_2H_2:H_2 = 1:30, N_2 balance, see Table 5). It is labelled as 'high conversion conditions' in the experiment to distinguish from 'low conversion conditions', since two catalyst plates are applied and N_2 dilution is lower compared to another set of tests. The operating temperatures were set to 30 °C and 50 °C. The working pressure was set to 1 bar.

For precise assessment of low-temperature hydrogenation activity of Pd, conditions yielding only low conversion rates were chosen afterwards, achieving homogenous product concentration over the catalytic plate. Therefore, one catalyst plate was replaced by a blind Si substrate, and the tests were labelled as 'low conversion conditions' in Table 5. The total flow rate was increased to 134 ml/min (with 2.67 % of acetylene) while the ratio decreased to C_2H_2:H_2 = 1:10 (N_2 balance). These conditions yielded conversion rates low enough to validate the reaction model. For this validation, the temperature was varied between 19.5 and 50 °C.

For each operating temperature, the measurement was repeated five times of which each period takes about 20 min. C_2H_2 conversion, selectivity of C_2H_2 and C_2H_4 in the experiments was calculated as

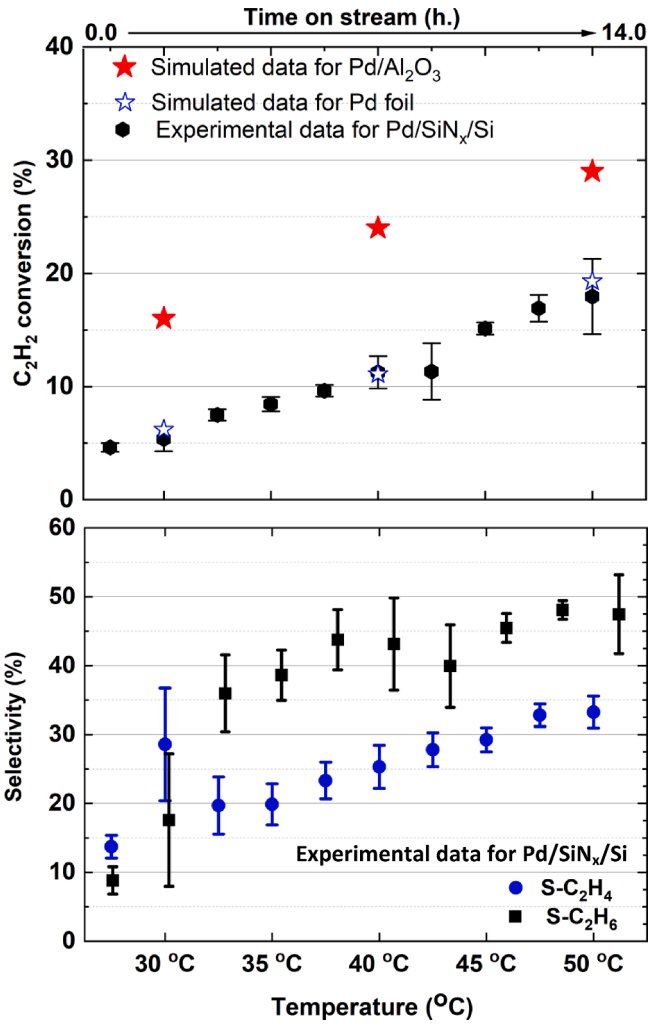

Fig. 7. (Top) Conversion and (Bottom) selectivity of the reaction as functions of temperature. Simulated data for Pd/Al_2O_3 and Pd foil are also displayed for comparison. Simulations were done at the same condition of catalytic test for the low conversion cases (Table 5) and with only one catalyst plate.

follows:

$$\chi_{C_2H_2} = \frac{n_{C_2H_{2,in}} - n_{C_2H_{2,out}}}{n_{C_2H_{2,in}}} \quad (8)$$

$$S_{C_2H_4} = \frac{n_{C_2H_{4,out}}}{n_{C_2H_{2,in}} - n_{C_2H_{2,out}}} \quad (9)$$

where n denotes the molar amounts of the gases in the subscript.

5. Result and discussion

5.1. Reactor design visualization

As shown in Fig. 3, the nozzle configuration plays an important role in controlling the gas flow inside the reactor. The streamlines in the reactor are described for three different nozzle geometries. One can see that for single and triple circular nozzles, a region of turbulent flow can be observed near the inlet. The effect of nozzle geometries is also estimated through the kinetic simulation, yielding a conversion of 19.8 % for one circular nozzle compared to 18.9 % for the slit nozzle. As described by these values, the influence of this turbulent region on the total conversion is rather small. In the laminar flow region of the reactor, relatively homogeneous distribution of gas velocities and concentration

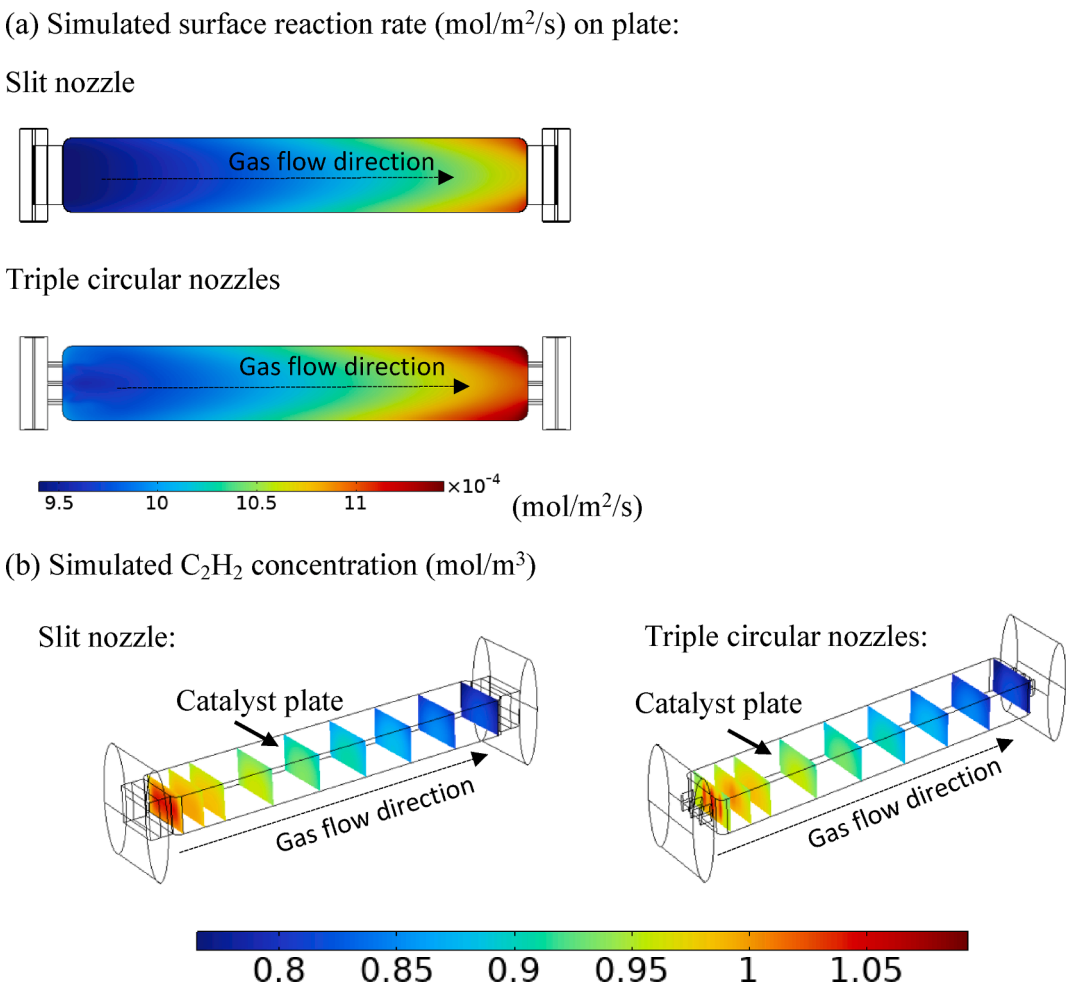

Fig. 8. (a) Simulated surface reaction rate on plate for the case of slit nozzle and triple circular nozzles using model for Pd foil. (b) 2D- planes of simulated C_2H_2 concentration displayed inside reactor. Simulations were done at the same condition of catalytic test for the low conversion case and at temperature of 50 °C. Only one catalyst plate was taken in this simulation. The catalyst plate is on the top and the z direction is scale to 5 times for clarification.

is established, which supports similar reaction rates in the whole region (see Fig. 8). Therefore, to achieve the design goal: both high efficiency and homogenous reaction inside reactor, the triple circular nozzles configuration was chosen for the device.

The same rule is applied to select the nozzle diameter. As shown in Fig. 3(b), the smaller the nozzle diameter is, the higher velocity at the inlet and larger the turbulent region will be. When the nozzle diameter equals to the channel width (1 mm), turbulences are only observed at the corners of the reactor at the inlet side. For ease of manufacturing the prototype, the dimension of the nozzle size was fixed to 0.5 mm for the prototype.

We also investigated the influence of the height between the catalyst plates on the flow patterns established in the reactor. As seen in Fig. 4, the extension of the turbulent flow region is strongly dependent on this parameter. The turbulent region is shorter for smaller channels, yielding a significantly larger area with homogeneous flow properties. The flow velocity profile also demonstrates that velocity is mainly constant along the reactor in the laminar flow region. However, there is a trade-off between reducing the space and the pressure drop occurring along the channel. Since there is no significant difference in the length of turbulent regime for channel heights of 0.7 and 1 mm, a height of 1 mm was chosen. The prototype is displayed in Fig. 2.

5.2. Characterization of reactor performance

5.2.1. Pressure drop experiment and modelling

As shown in Fig. 5, the pressure drop in the reactor increases as the standard flow rate of the feed gas increases and the working pressure decreases. This is because both the increase of the standard flow rate and the decrease of the working pressure result in the increase the actual volumetric flow and consequently a rise of pressure drop in the reactor. However, very low pressure drops in the mbar range were observed for all operating pressures even at very high flow rates of up to 350 ml/min. Experimental and model data follow the same trend and pressure ranges. The remaining difference between experimental and theoretical values of 5 mbar for the worst case of 360 ml/min and 0.5 bar working pressure (corresponding to a deviation of 1 %) is most likely caused by small variations in size of the real device or accuracy limits of the pressure gauges used. To illustrate this, we simulated the pressure drop with a nozzle diameter of 0.4 mm, in addition. One can see that the experimental values lie between the simulation data for nozzle diameters of 0.4 and 0.5 mm, which is consistent with the given explanation.

Following the depicted trend in detail in Fig. 5, one can see that the curves are divided into two regions: at low flow rates an exponential dependence of pressure drop on flow rate is observed meanwhile at high flow rate, where turbulent flow is dominant, pressure drop increases linearly with flow rate. This observation is in good agreement with the basics of fluid dynamics, which is also illustrated by the simulated flow rates, as displayed in Fig. 5 (right). For low flow rates, such as 30 ml/

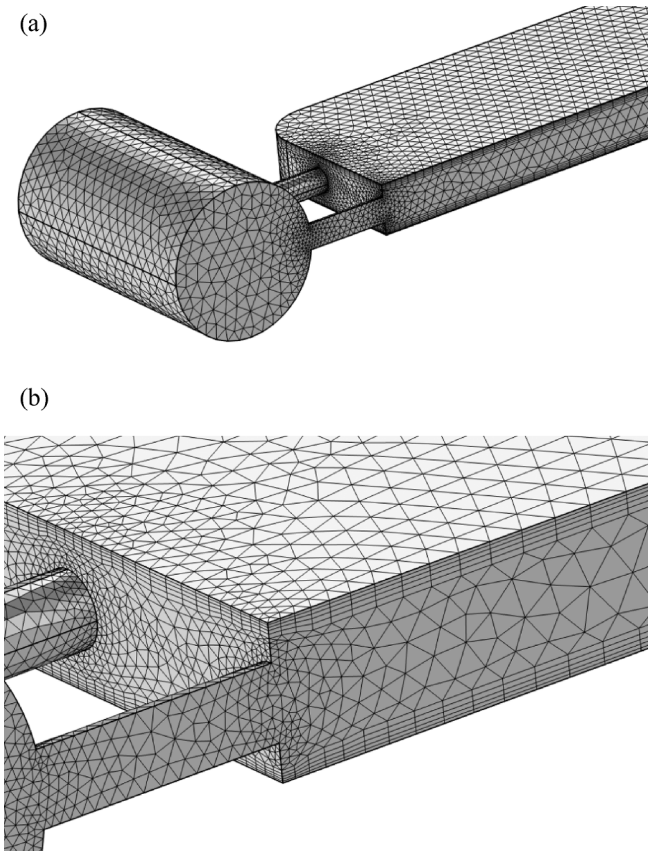

Fig. A1. Mesh of simulation model. (a) Clip view from the middle of the flow direction; (b) Enlarge view of the boundary layers.

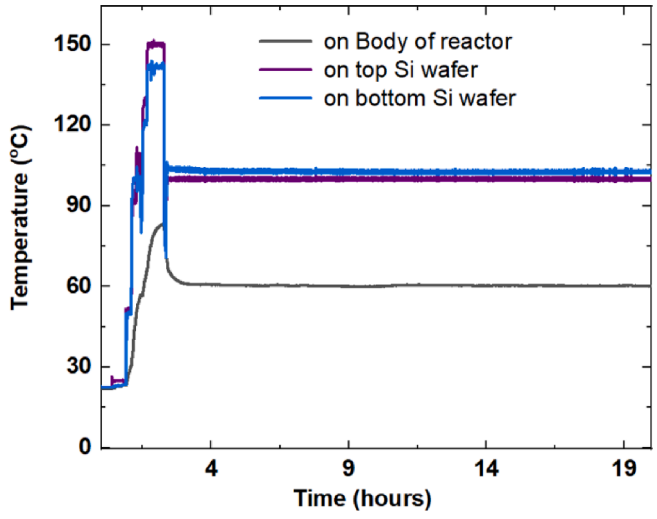

Fig. A2. Temperature profiles during one experimental test within 20 h. The body of the reactor, the top and the bottom Si wafers were first heated up, then adjusted to the targeted temperature: 60 °C for the reactor body, 100 °C for the top and the bottom Si wafers with 2 °C difference.

min, laminar flow is dominant. When gas flow rate increases, turbulences form 5–10 mm near the gas inlet, (Fig. 5, right). Due to inhomogeneous reaction conditions in these regions, these areas can be identified on the sample after catalytic testing (as Fig. 6(b)).

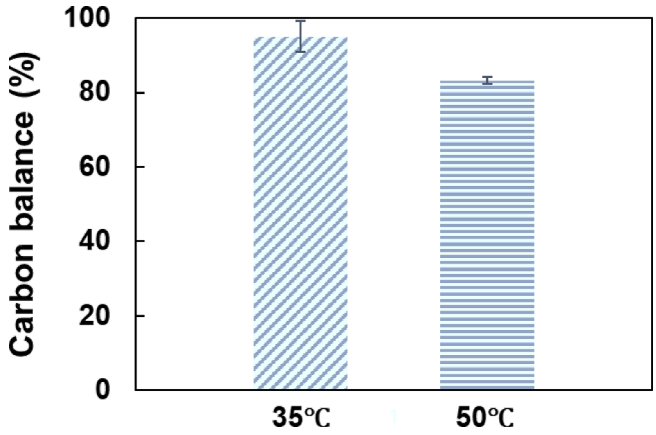

Fig. A3. Carbon balance for the high conversion cases.

5.2.2. Direct current electrical heating

The direct current (DC) electrical heating was experimentally investigated for the reactor prototype. The DC source was applied to the catalyst plate via spring loaded connectional pins, as shown in Fig. 2. After applying electric power, the temperature increased rapidly to set temperature (100 °C) and remained stable for a testing time of more than 20 h, as shown in Fig. A2. For the case of symmetric heating (top and bottom catalyst plate in series connection) the temperatures were almost identical on both plates (2 °C difference, see Fig. A2). For the asymmetric case (only one catalyst plate connected to the current source), a difference of 20 °C was observed. The temperature of the reactor housing amounted to 60 °C for both cases. In this work, a total power of only 6 W was needed to achieve a temperature of 100 °C at the catalyst plates. This low power demand can be even reduced by implementing a thin-film heater concept as described by Kwon et al. [42] in future.

5.2.3. Catalytic activity

Finally, we report on the first catalytic test using acetylene hydrogenation as model reaction, and ethylene and ethane were quantified by GC analysis. Fig. 6(a) shows the conversion and selectivity profile in the prototype reactor loaded with two catalyst wafers at two different operating temperatures 35 °C and 50 °C (tests at 'high conversion condition' in Table 5). One can see that the conversion reaches nearly 100 % at 50 °C but only yields very low selectivity, i.e., around 25 %. For the 35 °C case the selectivity of C_2H_4 is around 70 %. In addition, some oligomers were formed, and green oil was observed on the surface as well, shown in Fig. 6(b). This observation is consistent with those in references [32,33,43,44], where acetylene hydrogenation took place in the presence of ethylene on Pd black and Pd/Al_2O_3 catalysts, resulting in a deficit in the carbon balance (see Fig. A3). These observations suggest that hydrogenation of acetylene using Pd/SiN_x catalyst also oligomerizes acetylene the same as Pd black and Pd/Al_2O_3 catalysts.

The results of the full temperature series for tests at 'low conversion condition' with one catalyst wafer (see Table 5) are depicted in Fig. 7(a) and compared to the previously described reaction models for Pd/γ-Al_2O_3 and Pd foil in simulation. The experimental data obtained for the Pd/SiN_x/Si samples used in this study are in close agreement with the simplified power low model for a Pd foil, suggesting a good coupling of the simulation model with the real reactor as proposed in the design criteria. However, more investigations are still needed to obtain additional experimental data to enhance the accuracy and reliability of the kinetic modelling.

As shown in Fig. 7(b), selectivity of both C_2H_4 and C_2H_6 increases with temperature. This trend was also observed for a Pd(1 1 1) catalyst in some studies [38,39]. For Pd on supports such as Al_2O_3, TiO_2 and SiC, low temperature is in favour of the oligomerization [45,46]. The

formation of C_2 coupling products such as benzene and other oily products are known and intensively studied, and are, at this point, not of interest in the reactor cell development aimed for general catalytic applications.

Fig. 8(a) shows the spatially resolved simulated reaction rate in the reactor at 50 °C for a slit nozzle and triple circular nozzles applying the power law rate equation derived from Pd foil experiments [38,39]. In general, one can see for both designs that the reaction rate increases along the reactor axis. This is to be expected, due to the negative reaction order of acetylene and the excess of hydrogen in the feed. While the consumption of acetylene results in a significant increase of the reaction rate with increased conversion, the concentration change of hydrogen is negligible. In case of triple circular nozzles, higher reaction rates can be achieved compared to the slit nozzle case, which in good agreement with the previously discussed phenomena. At regions near inlet nozzles, feed gases move with higher velocity causing significant turbulences and backmixing (see Fig. 5). The backmixing causes a local decrease of the acetylene concentration (Fig. 8b) resulting in a higher reaction rate due to its negative order in the power law rate equation. In the radial direction, the reaction rate is lower at the centre of plate, which agrees with the C_2H_2 concentration showed in Fig. 8(b), in which more C_2H_2 gas is consumed near edge regions due to lower velocity here. As shown in Fig. 8(b), for all the planes, the radial C_2H_2 concentration distribution is quite homogeneous (2 % deviation), which demonstrate that the reactor fulfils the requirement of design concepts, as mentioned in the section Concept and Design rules, enabling fast catalytic characterization of materials and adaption to other reaction conditions and a variety of applications (e.g., operando spectroscopic studies).

6. Conclusion

A reactor cell and virtual replica were presented that are suitable for comprehensively testing the properties of thin film catalysts. The design was visualized by CFD simulation and characterized by experimental and numerical models to achieve additional insight in reactor operation. The virtual replica on the other hand allows to determine the gas flow profile and assess operation parameter limits under which homogeneous conditions are maintained inside the reactor. The direct current electrical heating concept allows for a fast and accurately controlled temperature during reaction. Due to the fast response, temperature deviations can be compensated quickly. Further advantage of direct current electrical heating is not only the low power consumption but also the flexibility and mobility of the reactor cell in assembly with measurement systems. A first catalytical test with acetylene hydrogenation as model reaction and thin-film palladium catalyst plates showed reasonable results in agreement with model predictions. Operating conditions can be adapted to enable fast kinetic studies as demonstrated. The reactor is designed to enable fast catalytic characterization of materials and can be adapted to a variety of applications. The virtual replica established by the multiphysics model enables in-depth understanding of the obtained catalytical data and allows comprehensive parameter studies to find optimized process parameters without the need of large amounts of catalyst samples.

Declaration of Competing Interest

The authors declare the following financial interests/personal relationships which may be considered as potential competing interests: All reports financial support was provided by Federal Ministry of Education and Research Berlin Office.

Data availability

No data was used for the research described in the article.

Acknowledgements

The authors acknowledge support from the German Federal Ministry of Education and Research in the framework of the project CatLab (03EW0015A/B), Manuela Arztmann, Alexander Steigert for catalyst preparation.

Appendix

The mesh was first generated by Physics-Controlled Mesh Method, then was refined by using boundary layer mesh at two catalyst plates, resulting in total 555 468 domain elements and 66 552 boundary elements.

Pre-estimation for sensitivity of the mesh by changing the numbers of boundary layers from 0, 5 and 10 was carried out. Less than 1 % of validation results between 5 and 10 layers were observed. Therefore, 5 boundary layers was chosen, as shown in Fig. A1.

The direct current electrical heating concept benefits our reactor cell and its virtual replica including: 1) fast and accurately controlled temperature during reaction, 2) low power consumption, 3) the flexibility and mobility of the reactor cell in assembly with measurement systems, 4) and possible adaptions to a variety of applications (operando spectroscopic studies).

As shown in Fig. A2, after applying electric power, the temperature increased rapidly to set temperature and remained stable for a testing time of more than 20 h, and the temperatures of the top and bottom Si wafers were almost identical.

Carbon balance was conducted as shown in Fig. A3. Apart from ethylene and ethane mentioned in the main text, C4 and other products were estimated. Carbon balance below 1 means that there are many other higher C_xH_y in addition to C_2H_4, C_2H_6 and C_4H_{10}.

References

[1] Best Research-Cell Efficiency Chart, (n.d.). https://www.nrel.gov/pv/cell-efficiency.html.
[2] https://www.pv-magazine.com/2022/01/21/chinese-pv-industry-may-reach-500-gw-module-capacity-by-year-end/.
[3] R. Schlögl, B. Rech, CatLab: Hydrogen and beyond - Thin-film catalysts for sustainable chemistry with renewable electricity, (2022). https://doi.org/10.26125/RABF-VW12.
[4] M.I. Domínguez, M.A. Centeno, M. Martínez T., L.F. Bobadilla, Ó.H. Laguna, J. A. Odriozola, Current scenario and prospects in manufacture strategies for glass, quartz, polymers and metallic microreactors: a comprehensive review, Chem. Eng. Res. Des. 171 (2021) 13–35, https://doi.org/10.1016/j.cherd.2021.05.001.
[5] V. Meille, Review on methods to deposit catalysts on structured surfaces, Appl. Catal. A 315 (2006) 1–17, https://doi.org/10.1016/j.apcata.2006.08.031.
[6] M.J. Ndolomingo, N. Bingwa, R. Meijboom, Review of supported metal nanoparticles: synthesis methodologies, advantages and application as catalysts, J. Mater. Sci. 55 (2020) 6195–6241, https://doi.org/10.1007/s10853-020-04415-x.
[7] S. Mehla, J. Das, D. Jampaiah, S. Periasamy, A. Nafady, S.K. Bhargava, Recent advances in preparation methods for catalytic thin films and coatings, Catal. Sci. Technol. 9 (2019) 3582–3602, https://doi.org/10.1039/C9CY00518H.
[8] S. Biran Ay, N. Kosku Perkgoz, Nanotechnological advances in catalytic thin films for green large-area surfaces, J. Nanomater. 2015 (2015), 257547, https://doi.org/10.1155/2015/257547.
[9] Y. Chin, J. Hu, C. Cao, Y. Gao, Y. Wang, Preparation of a novel structured catalyst based on aligned carbon nanotube arrays for a microchannel Fischer-Tropsch synthesis reactor, Catal. Today 110 (2005) 47–52, https://doi.org/10.1016/j.cattod.2005.09.007.
[10] G.M. Arzac, A. Fernández, V. Godinho, D. Hufschmidt, M.C. Jiménez de Haro, B. Medrán, O. Montes, Pd-C catalytic thin films prepared by magnetron sputtering for the decomposition of formic acid, Nanomaterials 11 (2021) 2326, https://doi.org/10.3390/nano11092326.
[11] M. Sasaki, H. Hamada, Y. Kintaichi, T. Ito, A new low-pressure flow type reactor system for the study of catalysis over thin films: N2O decomposition over CoAg binary metal thin films, Appl. Catal. A 159 (1997) 21–31, https://doi.org/10.1016/S0926-860X(97)00037-9.
[12] J.P. Holgado, J. Morales, A. Caballero, A.R. González-Elipe, Plate reactor for testing catalysts in the form of thin films, Appl Catal B 31 (2001) L5–L10, https://doi.org/10.1016/S0926-3373(01)00143-6.
[13] K. Venkataraman, J.M. Redenius, L.D. Schmidt, Millisecond catalytic wall reactors: dehydrogenation of ethane, Chem. Eng. Sci. 57 (2002) 2335–2343, https://doi.org/10.1016/S0009-2509(02)00132-X.

[14] A. Ates, P. Pfeifer, O. Görke, Thin-film catalytic coating of a microreactor for preferential co oxidation over pt catalysts, Chem. Ing. Tech. 85 (2013) 664–672, https://doi.org/10.1002/cite.201200166.
[15] J. Aubin, L. Prat, C. Xuereb, C. Gourdon, Effect of microchannel aspect ratio on residence time distributions and the axial dispersion coefficient, Chem. Eng. Process. 48 (2009) 554–559, https://doi.org/10.1016/j.cep.2008.08.004.
[16] S. Hwang, O. Kwon, S. Ahn, J. Kim, Silicon-based micro-reactor for preferential CO oxidation, Chem. Eng. J. 146 (2009) 105–111, https://doi.org/10.1016/j.cej.2008.08.037.
[17] M. Bhattacharya, M.P. Harold, V. Balakotaiah, Shape normalization for catalytic monoliths, Chem. Eng. Sci. 59 (2004) 3737–3766, https://doi.org/10.1016/j.ces.2004.02.020.
[18] C. Junaedi, K. Hawley, D. Walsh, S. Roychoudhury, M. Abney, J. Perry, Compact and Lightweight Sabatier Reactor for Carbon Dioxide Reduction, in: 41st International Conference on Environmental Systems, American Institute of Aeronautics and Astronautics, Portland, Oregon, 2011. https://doi.org/10.2514/6.2011-5033.
[19] P. Avila, M. Montes, E.E. Miró, Monolithic reactors for environmental applications, Chem. Eng. J. 109 (2005) 11–36, https://doi.org/10.1016/j.cej.2005.02.025.
[20] C. Koutsodontis, A. Hammad, M. Lepage, Y. Sakamoto, G. Fóti, C.G. Vayenas, Electrochemical promotion of no reduction by c2h4 in excess o2 using a monolithic electropromoted reactor and pt–rh sputtered electrodes, Top. Catal. 50 (2008) 192–199, https://doi.org/10.1007/s11244-008-9110-3.
[21] S. Balomenou, D. Tsiplakides, A. Katsaounis, S. Thiemann-Handler, B. Cramer, G. Foti, C.h. Comninellis, C.G. Vayenas, Novel monolithic electrochemically promoted catalytic reactor for environmentally important reactions, Appl Catal B 52 (2004) 181–196, https://doi.org/10.1016/j.apcatb.2004.04.007.
[22] S. Srinivas, A. Dhingra, H. Im, E. Gulari, A scalable silicon microreactor for preferential CO oxidation: performance comparison with a tubular packed-bed microreactor, Appl. Catal. A 274 (2004) 285–293, https://doi.org/10.1016/j.apcata.2004.07.012.
[23] K.F. Jensen, Microreaction engineering — is small better? Chem. Eng. Sci. 56 (2001) 293–303, https://doi.org/10.1016/S0009-2509(00)00230-X.
[24] X. Ouyang, R.S. Besser, Development of a microreactor-based parallel catalyst analysis system for synthesis gas conversion, Catal. Today 84 (2003) 33–41, https://doi.org/10.1016/S0920-5861(03)00298-0.
[25] N. Engelbrecht, S. Chiuta, R.C. Everson, H.W.J.P. Neomagus, D.G. Bessarabov, Experimentation and CFD modelling of a microchannel reactor for carbon dioxide methanation, Chem. Eng. J. 313 (2017) 847–857, https://doi.org/10.1016/j.cej.2016.10.131.
[26] S.R.L. Gobert, S. Kuhn, L. Braeken, L.C.J. Thomassen, Characterization of Milli- and microflow reactors: mixing efficiency and residence time distribution, Org. Process Res. Dev. 21 (2017) 531–542, https://doi.org/10.1021/acs.oprd.6b00359.
[27] O. Levenspiel, Chemical reaction engineering, 3rd ed, Wiley, New York, 1999.
[28] COMSOL Multiphysics Reference Manual, version 5.3, (2020). www.comsol.com.
[29] W. Fulkerson, J.P. Moore, R.K. Williams, R.S. Graves, D.L. McElroy, Thermal conductivity, electrical resistivity, and seebeck coefficient of silicon from 100 to 1300°K, Phys. Rev. 167 (1968) 765–782, https://doi.org/10.1103/PhysRev.167.765.
[30] N.M. Ravindra, B. Sopori, O.H. Gokce, S.X. Cheng, A. Shenoy, L. Jin, S. Abedrabbo, W. Chen, Y. Zhang, Emissivity measurements and modeling of silicon-related materials: an overview, Int. J. Thermophys. 22 (2001) 1593–1611, https://doi.org/10.1023/A:1012869710173.
[31] A. Pachulski, R. Schödel, P. Claus, Kinetics and reactor modeling of a Pd-Ag/Al2O3 catalyst during selective hydrogenation of ethyne, Appl. Catal., AGeneral. 445–446 (2012) 107–120, https://doi.org/10.1016/j.apcata.2012.08.018.
[32] A. Borodziński, A. Cybulski, The kinetic model of hydrogenation of acetylene–ethylene mixtures over palladium surface covered by carbonaceous deposits, Appl. Catal. A 198 (2000) 51–66, https://doi.org/10.1016/S0926-860X(99)00498-6.
[33] A.N.R. Bos, K.R. Westerterp, Mechanism and kinetics of the selective hydrogenation of ethyne and ethene, Chem. Eng. Process. 32 (1993) 1–7, https://doi.org/10.1016/0255-2701(93)87001-B.
[34] L.Z. Gva, K.E. Kho, Kinetics of acetylene hydrogenation on palladium deposited on alumina, Kinet. Catal. (engl. Transl.); (united States). 29 (2) (1988). https://www.osti.gov/biblio/6334769.
[35] N.A. Khan, S. Shaikhutdinov, H.-J. Freund, Acetylene and ethylene hydrogenation on alumina supported pd-ag model catalysts, Catal. Lett. 108 (2006) 159–164, https://doi.org/10.1007/s10562-006-0041-y.
[36] V.A. Men'shchikov, Y.G. Fal'kovich, M.E. Aerov, Hydrogenation kinetics of acetylene on a palladium catalyst in the presence of ethylene, Kinet. Catal. (USSR) (engl. Transl.); (united States). 16 (6) (1976). https://www.osti.gov/biblio/7134349.
[37] C. Urmès, J.-M. Schweitzer, A. Cabiac, Y. Schuurman, Kinetic study of the selective hydrogenation of acetylene over supported palladium under tail-end conditions, Catalysts 9 (2019) 180, https://doi.org/10.3390/catal9020180.
[38] H. Molero, B.F. Bartlett, W.T. Tysoe, The hydrogenation of acetylene catalyzed by palladium: hydrogen pressure dependence, J. Catal. 181 (1999) 49–56, https://doi.org/10.1006/jcat.1998.2294.
[39] D. Mei, P. Sheth, M. Neurock, C. Smith, First-principles-based kinetic Monte Carlo simulation of the selective hydrogenation of acetylene over Pd(111), J. Catal. 242 (2006) 1–15, https://doi.org/10.1016/j.jcat.2006.05.009.
[40] A.N.R. Bos, E.S. Botsma, F. Foeth, H.W.J. Sleyster, K.R. Westerterp, A kinetic study of the hydrogenation of ethyne and ethene on a commercial Pd/Al2O3 catalyst, Chem. Eng. Process. 32 (1993) 53–63, https://doi.org/10.1016/0255-2701(93)87006-G.
[41] R.J. Kee, M.E. Coltrin, P. Glarborg, H. Zhu, Chemically reacting flow: theory, modeling, and simulation, Wiley (2017), https://doi.org/10.1002/9781119186304.
[42] O.J. Kwon, S.-M. Hwang, J.-G. Ahn, J.J. Kim, Silicon-based miniaturized-reformer for portable fuel cell applications, J. Power Sources 156 (2006) 253–259, https://doi.org/10.1016/j.jpowsour.2005.06.024.
[43] S. Leviness, V. Nair, A.H. Weiss, Z. Schay, L. Guczi, Acetylene hydrogenation selectivity control on PdCu/Al2O3 catalysts, J. Mol. Catal. 25 (1984) 131–140, https://doi.org/10.1016/0304-5102(84)80037-1.
[44] A. Sárkány, L. Guczi, A.H. Weiss, On the aging phenomenon in palladium catalysed acetylene hydrogenation, Appl. Catal. 10 (1984) 369–388, https://doi.org/10.1016/0166-9834(84)80131-1.
[45] Y. Cao, Z. Sui, Y. Zhu, X. Zhou, D. Chen, Selective hydrogenation of acetylene over pd-in/al $_{2\ o}$ 3 catalyst: promotional effect of indium and composition-dependent performance, ACS Catal. 7 (2017) 7835–7846, https://doi.org/10.1021/acscatal.7b01745.
[46] Z. Guo, Y. Liu, Y. Liu, W. Chu, Promising SiC support for Pd catalyst in selective hydrogenation of acetylene to ethylene, Appl. Surf. Sci. 442 (2018) 736–741, https://doi.org/10.1016/j.apsusc.2018.02.145.